European Journal of Mechanics / B Fluids 70 (2018) 36–45

Contents lists available at ScienceDirect

European Journal of Mechanics / B Fluids

journal homepage: www.elsevier.com/locate/ejmflu

Wall collision of deformable bubbles in the creeping flow regime

Fabian Denner

Department of Mechanical Engineering, Imperial College London, London, SW7 2AZ, United Kingdom

ARTICLE INFO

Article history:
Received 19 April 2017
Received in revised form 25 October 2017
Accepted 13 February 2018
Available online 19 February 2018

Keywords:
Bubble–wall collision
Bubble deformation
Film drainage
Creeping flow
Viscocapillary balance

ABSTRACT

A systematic study of the hydrodynamic mechanisms governing the collision of a rising bubble with a solid wall in the creeping flow regime (Re $<$ 1) is presented, using direct numerical simulation. The presented results reveal self-similar aspects of the bubble–wall collision with respect to the capillary number, in particular of the film between the bubble and the wall as well as of the deformation and shape of the bubble. This similarity holds despite the extreme deformation of the bubble in some of the considered cases and is shown to be independent of the approach velocity and the fluid properties, indicating that the collision of a bubble with a solid wall in the creeping flow regime is governed by the balance of viscous stresses and surface tension, while the inertia of the bubble has a negligible influence. The timescale associated with the drainage of the film separating the bubble surface and the wall is also related to the viscocapillary balance, and is found to be independent of the size of the bubble. An empirical correlation is proposed based on the presented results to a priori estimate the drainage time of this film. Because the behaviour of a bubble during film drainage is quasi-stationary, the findings associated with film drainage also apply to bubble–wall collisions outside the remit of the creeping flow regime (Re $\gg$ 1).

1. Introduction

The collision of bubbles with solid walls or particles plays an important role in various natural phenomena and engineering application, such as the formation of foams [1–3] (or similarly emulsions), froth flotation [4] or the enhancement of convective heat transfer [5,6]. In the past two decades a number of experimental and numerical studies have unravelled some of the dominating mechanisms and characterising parameters governing the hydrodynamics of the collisions of bubbles with solid walls [6–16]. As a bubble approaches and collides with a wall, the kinetic energy of the bubble has to be dissipated, a process which is dominated by two hydrodynamic mechanisms [3,9]: (a) an increase in surface energy due to deformation of the bubble, and (b) drainage of the film separating the bubble surface and the wall.

If the kinetic energy of the bubble is sufficiently high, the bubble bounces off the wall a number of times, indicating that the energy transfer between surface energy and kinetic energy is faster than the dissipation in the film between the bubble and the wall [3,9,10]. The dissipation in this film becomes the dominant hydrodynamic mechanism once the kinetic energy is sufficiently low [1]. In experiments reported by Tsao and Koch [7], the collision of a bubble with Re $=$ 420 (the Reynolds number Re is formally defined in Section 2) with a solid wall was found to be almost fully elastic, with approximately 95% of the surface energy being transferred back into kinetic energy during the first bounce. Tsao and Koch [7] further suggested that the dissipation of energy is strongly influenced by a separation of the boundary layer from the wall of impact when the bubble bounces off that wall as well as by acoustic radiation due to high frequency oscillations of the bubble. In fact, Krzan et al. [17] and Malysa et al. [8] reported experimental measurements with bubbles oscillating at a frequency of $f > 1000$ s^{-1} as the bubble moved away from the wall after the first bounce. Numerical simulations by Albadawi et al. [13] indicate that these oscillations are predominantly driven by pressure fluctuations as a result of the rapid filling of the film separating the bubble and the wall as the bubble moves away from the wall. Legendre et al. [18] and Zenit and Legendre [10] devised a coefficient of restitution for bubbles bouncing off a wall using a modified Stokes number, based on the mass and added mass of the bubble during collision.

In cases where the kinetic energy of the bubble is too low, the bubble is not bouncing off the wall [19] and the film drains until rupture and the formation of triple phase contact. In special cases, such as the collision of a bubble with a superhydrophilic surface (*i.e.* contact angle of $\alpha \to 0°$), the film can stabilise before reaching its critical rupture thickness [12,13,15]. Rupture of this film usually occurs when the attractive forces due to van der Waals interaction (typically described as a disjoining pressure) become dominant, at a film thickness of $h \lesssim 10^{-7}$ m [11,20–23]. Ruckenstein and Sharma [24] highlighted the fact that surface waves increase the drainage of the film for large film radii. Experimental

E-mail address: f.denner09@imperial.ac.uk.

https://doi.org/10.1016/j.euromechflu.2018.02.002

results reported by Parkinson and Ralston [25] of an air bubble rising in water with Re $<$ 1 and colliding with a solid wall, for which the deformation of the bubble is negligible even during wall collision, showed the drainage time of the film to increase with increasing bubble size as a result of the larger buoyancy force. Even for cases with large bubble Reynolds number (Re $\gg$ 1), the Reynolds number of the film is small, typically $\mathrm{Re_f} \ll 1$. The film drainage and its effect on the bubble has, hence, often been studied using lubrication theory [11,14,16,26–30]. Zenit and Legendre [10] proposed that the dominating mechanism for the drainage of the film is the inertia of the fluid, with viscosity being only important at very small film thickness. This stands somewhat in contradiction to findings reported by Sanada et al. [1] that showed a significant influence of viscosity on the film drainage for the collision of bubbles with a free surface. Zawala et al. [3] suggested that the radius of the film is the parameter dominating the coalescence time, with a larger film radius resulting in a longer time required for the film to drain. Similar conclusions have been drawn in a number of other publications studying the collision of a bubble with a solid wall [13,18], with a free surface [1] and with another bubble [31].

Research efforts with respect to bubble–wall collisions have so far focused predominantly on bubbles with moderate to high Reynolds number (Re $\gg$ 1) and, in particular, on the dynamic bouncing behaviour of bubbles colliding with solid walls and free surfaces. Previous studies of the collision of bubbles with a solid wall or a free surface in the creeping flow regime (Re $<$ 1) have typically assumed a negligible interface deformation [25,30,32], which is a reasonable assumption for air bubbles in water [25,30] and which simplifies the theoretical analysis. This assumption has previously been utilised, for instance, by Parkinson and Ralston [25] for bubble–wall collisions, Ascoli et al. [33] for the collision of a drop with a rigid wall and by Abid and Chesters [32] for drop–drop collisions. However, the collision of a bubble with a solid wall in the creeping flow regime for two-phase systems that allow a significant deformation of the bubble during collision, such as an air bubble in glycerol, lubricant oil or molten glass as well as many liquid–liquid flows, has not been considered to date. In such a case the significant interface deformation (*e.g.* dimple formation) during the collision of the bubble with a solid wall means the solution is nonlinear [34] and, hence, complicates a theoretical analysis. For oscillating drops, which hydrodynamically can be regarded as a closely related problem, Becker et al. [35] observed that nonlinear effects become important for an oscillation amplitude of $>$ 10%. Similarly, the dispersion and viscous attenuation of capillary waves becomes significantly affected by the wave amplitude if the initial amplitude of the capillary wave is $\gtrsim$ 5% of the wavelength [36]. Thus, the nonlinearity introduced by the interface deformation cannot be neglected for an accurate determination and quantification of the governing mechanisms of a bubble–wall collision when the deformation of the bubble is significant, even in the creeping flow regime.

In this article, a systematic numerical study of the collision of a single gravity-driven bubble with a solid wall in the creeping flow regime (Re $<$ 1) is presented, based on direct numerical simulations (DNS) that resolve all relevant length and time scales of the entire two-phase system using a state-of-the-art finite volume framework for interfacial flows [37,38]. The computational setup is schematically shown in Fig. 1 and further discussed in Section 3.2. The presented results reveal a self-similar temporal evolution of the bubble–wall collision with respect to the capillary number Ca (formally defined in Section 2), which compares viscous stresses to surface tension, both for the film thickness separating the bubble surface from the wall as well as the shape of the bubble. This self-similarity is observed for all considered fluid properties, despite the nonlinearity introduced by the considerable deformation of the fluid interface, and is shown to be independent of the approach velocity of the bubble. Furthermore, the drainage of the film between the bubble and the wall is also governed by the balance of viscous stresses and surface tension, and a similar temporal evolution of the film thickness with respect to the characteristic timescale of the film drainage is observed for all considered cases. This allows an a priori approximation of the time required for the film to drain to its rupture thickness.

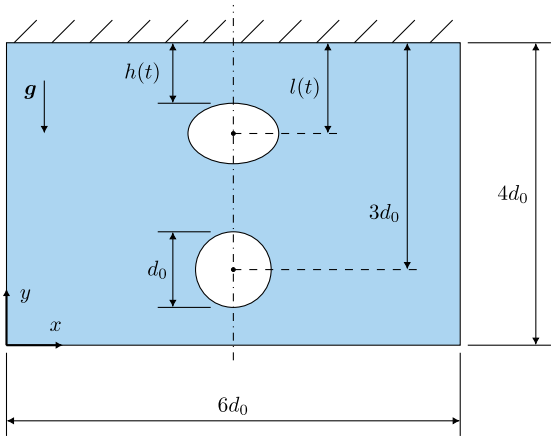

Fig. 1. Schematic two-dimensional illustration of a bubble colliding with a wall in the considered three-dimensional domain (shown is a slice in the symmetry plane with respect to the x and y coordinate axes), including relevant dimensions and notations, with h being the thickness of the film between the bubble and the wall and l being the distance between the centre of mass of the bubble and the wall.

In Section 2 the parametrisation of the bubble and the bubble–wall collision is devised. Subsequently, the applied numerical methodology and the setup of the numerical experiments are introduced in Section 3. The results are presented and analysed in Section 4, and the findings of this study are summarised and the article is concluded in Section 5.

2. Hydrodynamic parametrisation

The behaviour of bubbles is dominated by four physical mechanisms: buoyancy, inertia, viscous stresses and surface tension. Each of these four mechanisms can be quantified by their respective pressure scales, namely the buoyancy pressure $p_\mathrm{b} = g\,\Delta\rho\,d_0$, the dynamic pressure $p_\mathrm{dyn} = \rho_\mathrm{c}\,U^2$, the viscous pressure $p_\mu = \mu_\mathrm{c}\,U/d_0$, and the pressure due to surface tension $p_\sigma = \sigma/d_0$, where ρ is the density, μ is the dynamic viscosity, σ is the surface tension coefficient, subscript c denotes the continuous phase, subscript d denotes the dispersed phase, $\Delta\rho = \rho_\mathrm{c} - \rho_\mathrm{d}$, U is the characteristic velocity and d_0 is the initial diameter of the bubble. The characteristic velocity U of a freely rising bubble is defined as the terminal velocity of this bubble in an infinitely large domain under the sole action of gravity. In the creeping flow regime (Re $<$ 1) the characteristic velocity U follows directly from the balance of buoyancy and viscous stresses, given as [39]

$$U = \frac{g\,\Delta\rho\,d_0^2}{6\,\mu_\mathrm{c}\,\Lambda}, \tag{1}$$

with g being the gravitational acceleration and $\Lambda = (2+3\lambda)/(1+\lambda)$, where $\lambda = \mu_\mathrm{d}/\mu_\mathrm{c}$ is the viscosity ratio of the bulk phases.

The relative importance of the governing physical mechanisms of interfacial flows is typically described by the Reynolds number

$$\mathrm{Re} = \frac{p_\mathrm{dyn}}{p_\mu} = \frac{\rho_\mathrm{c}\,d_0\,U}{\mu_\mathrm{c}}, \tag{2}$$

which compares inertia to viscous effects, the capillary number

$$\mathrm{Ca} = \frac{p_\mu}{p_\sigma} = \frac{\mu_\mathrm{c}\, U}{\sigma} \tag{3}$$

which compares viscous forces and surface tension, and the Weber number

$$\mathrm{We} = \frac{p_\mathrm{dyn}}{p_\sigma} = \frac{\rho_\mathrm{c}\, d_0\, U^2}{\sigma} \tag{4}$$

which compares inertia and surface tension, with $\mathrm{We} = \mathrm{ReCa}$. Crucially, however, these three dimensionless groups neglect buoyancy. Hence, the Eötvös number Eo and the Morton number Mo are additionally used to parameterise the motion of bubbles. The Eötvös number is defined as

$$\mathrm{Eo} = \frac{p_\mathrm{b}}{p_\sigma} = \frac{g\, \Delta\rho\, d_0^2}{\sigma} \tag{5}$$

and compares the pressure scale of the bubble buoyancy to the pressure due to surface tension. The Morton number, given as

$$\mathrm{Mo} = \frac{p_\mathrm{b}\, p_\mu^4}{p_\mathrm{dyn}^2\, p_\sigma^3} = \frac{g\, \Delta\rho\, \mu_\mathrm{c}^4}{\rho_\mathrm{c}^2\, \sigma^3}, \tag{6}$$

represents a ratio of the influencing fluid properties and, conveniently, is not dependent on the size or the velocity of the bubble. As first demonstrated in the seminal work of Grace [40], the motion of a buoyancy-driven, freely rising bubble can be fully parameterised using the Reynolds number Re, the Eötvös number Eo and the Morton number Mo. Note that based on the characteristic velocity defined in Eq. (1), the buoyancy pressure in the creeping flow regime is $p_\mathrm{b} = 6\Lambda\, p_\mu$. Consequently, the Eötvös number in the creeping flow regime also follows as

$$\mathrm{Eo} = 6\,\Lambda\, \frac{p_\mu}{p_\sigma} = 6\,\Lambda\,\mathrm{Ca}. \tag{7}$$

From the characteristic velocity U follows the characteristic timescale (see e.g. [41])

$$t_\mathrm{c} = \frac{r_0}{U} = \frac{d_0}{2\,U}, \tag{8}$$

where $r_0 = d_0/2$ is the initial radius of the bubble, and the dimensionless time $\tau = t/t_\mathrm{c}$. With respect to the drainage of the film between the bubble and the wall, Chan et al. [27] proposed the timescale

$$t_\mathrm{f} = d_0 \sqrt{\frac{\mu_\mathrm{c}}{\sigma\, U}} = 2\, t_\mathrm{c}\, \sqrt{\mathrm{Ca}}, \tag{9}$$

which suggests that the balance of viscous stresses and surface tension is dominating the film drainage. A similar timescale for the drainage of such a film was proposed by Klaseboer et al. [31].

3. Numerical methodology

DNS of the entire three-dimensional two-phase system, including both bulk phases as well as the fluid interface, are conducted by resolving all relevant length and time scales. The dynamic behaviour of isothermal, Newtonian fluids in the incompressible flow regime is governed by the momentum equations

$$\rho\left(\frac{\partial u_i}{\partial t} + u_j \frac{\partial u_i}{\partial x_j}\right) = -\frac{\partial p}{\partial x_i} + \frac{\partial}{\partial x_j}\left[\mu\left(\frac{\partial u_i}{\partial x_j} + \frac{\partial u_j}{\partial x_i}\right)\right] + \rho\, g_i + f_{\sigma,i} \tag{10}$$

and the continuity equation

$$\frac{\partial u_i}{\partial x_i} = 0, \tag{11}$$

where $\boldsymbol{x} \equiv (x, y, z)$ denotes a Cartesian coordinate system, t represents time, $\boldsymbol{u}$ is the velocity, p is the pressure, $\boldsymbol{g}$ is the gravity vector and $\boldsymbol{f}_\sigma$ is the force due to surface tension acting at the fluid interface.

3.1. Numerical framework

The governing equations are solved numerically using a state-of-the-art finite-volume framework with collocated variable arrangement [37]. The momentum and continuity equations are solved for the primitive variables in a single linear system of equations, see Ref. [37] for details. The momentum equations, Eq. (10), are discretised using a second-order backward Euler scheme for the transient term, while the convection, diffusion and pressure terms are discretised using a central differencing scheme. The continuity equation, Eq. (11), is discretised using a balanced-force implementation of the momentum-weighted interpolation method, as proposed by Denner and van Wachem [37], which couples pressure and velocity.

The Volume-of-Fluid (VOF) method [42] is adopted to capture the interface between the immiscible fluids. The local volume fraction of both phases in each mesh cell is represented by the colour function γ, defined as $\gamma = 0$ in the continuous phase and $\gamma = 1$ in the dispersed phase, with the interface located in mesh cells with a colour function value of $0 < \gamma < 1$. The local density ρ and viscosity μ are defined as

$$\rho(\boldsymbol{x}, t) = \rho_\mathrm{c}\,[1 - \gamma(\boldsymbol{x}, t)] + \rho_\mathrm{d}\,\gamma(\boldsymbol{x}, t) \tag{12}$$

$$\mu(\boldsymbol{x}, t) = \mu_\mathrm{c}\,[1 - \gamma(\boldsymbol{x}, t)] + \mu_\mathrm{d}\,\gamma(\boldsymbol{x}, t), \tag{13}$$

respectively. Based on the underlying flow with velocity $\boldsymbol{u}$, the colour function γ is advected by the linear advection equation

$$\frac{\partial \gamma}{\partial t} + u_i \frac{\partial \gamma}{\partial x_i} = 0, \tag{14}$$

which is discretised using a compressive VOF method [38]. Assuming the force due to surface tension can be represented as a volume force acting in the interface region, the surface force per unit volume is described by the CSF model [43] as $\boldsymbol{f}_\sigma = \sigma\,\kappa\,\nabla\gamma$, where κ is the interface curvature.

Simulations conducted with this numerical framework for the dynamic behaviour of bubbles [38,41], and interfacial waves [36,44] have been shown to be in excellent agreement with analytical solutions, experimental data and numerical results reported in the relevant literature.

3.2. Setup of the numerical experiments

The collision of a single rising bubble with a solid wall is analysed using the DNS results of 18 different cases, the dimensionless properties for which are given in Table 1. The considered cases span a wide range of capillary numbers, density ratios and viscosity ratios for $\mathrm{Re} \leq 0.933$. For all presented results the reference time $t = 0$ is defined as the time at which the film thickness is $h = d_0/10$.

The three-dimensional computational domain of size $6d_0 \times 4d_0 \times 6d_0$, illustrated in Fig. 1, is represented by a Cartesian mesh with 470,400 cells. The bubble with diameter d_0 is initially situated in the centre of the domain with respect to the x-axis and the z-axis, at a distance $3d_0$ from the top wall, see Fig. 1. The bubble motion is induced by buoyancy only, the surface tension coefficient is assumed to be constant and mass transfer between the bulk phases as well as molecular forces (*e.g.* van der Waals forces) are neglected. At the top wall (*i.e.* the wall with which the bubble collides) a no-penetration/no-slip boundary condition is applied, and the computational mesh is gradually refined in the vicinity of this wall, with the computational node closest to the wall situated at a distance of $1.2 \times 10^{-3} d_0$ from the wall. The computational mesh is gradually coarsened towards the bottom and side walls, each of which is numerically treated as a free-slip wall. The applied time-step Δt corresponds to a Courant number of $\mathrm{Co} = |\boldsymbol{u}|\Delta t/\Delta x \leq 0.18$ and satisfies the capillary time-step criterion [45].

Table 1
Relevant dimensionless groups of the analysed bubbles colliding with a solid wall. A rising bubble is fully characterised by Re, Eo, Mo and μ_d/μ_c [40]. The capillary number Ca and the density ratio ρ_d/ρ_c are given here to provide a better overview of the considered parameter space.

Case	Ca	Re	Eo	Mo	ρ_d/ρ_c	μ_d/μ_c
A1	1	3.123×10^{-1}	1.206×10^{1}	1.235×10^{2}	0.001	0.01
A2	0.5	1.106×10^{-1}	6.033×10^{0}	1.235×10^{2}	0.001	0.01
A3	0.26	4.148×10^{-2}	3.139×10^{0}	1.235×10^{2}	0.001	0.01
B1	20	5.084×10^{-2}	2.412×10^{2}	3.732×10^{7}	0.99	0.01
B2	5	5.084×10^{-2}	6.030×10^{1}	5.832×10^{5}	0.99	0.01
B3	1	5.084×10^{-2}	1.206×10^{1}	4.665×10^{3}	0.99	0.01
B4	0.5	5.084×10^{-2}	6.030×10^{0}	5.832×10^{2}	0.99	0.01
B5	0.2	5.084×10^{-2}	2.412×10^{0}	3.732×10^{1}	0.99	0.01
B6	0.1	5.084×10^{-2}	1.206×10^{0}	4.665×10^{0}	0.99	0.01
C1	20	3.704×10^{-1}	2.457×10^{2}	7.164×10^{5}	0.1	0.05
C2	5	3.704×10^{-1}	6.143×10^{1}	1.119×10^{4}	0.1	0.05
C3	2	3.704×10^{-1}	2.457×10^{1}	7.164×10^{2}	0.1	0.05
C4	0.5	3.704×10^{-1}	6.143×10^{0}	1.119×10^{1}	0.1	0.05
C5	0.2	3.704×10^{-1}	2.457×10^{0}	7.164×10^{-1}	0.1	0.05
D1	0.5	2.082×10^{-1}	6.025×10^{0}	3.648×10^{1}	0.99	0.01
D2	0.5	2.603×10^{-2}	6.025×10^{0}	2.220×10^{3}	0.99	0.01
E1	20	9.328×10^{-1}	3.000×10^{2}	1.379×10^{5}	0.001	1.0
E2	0.2	9.328×10^{-1}	3.000×10^{0}	1.379×10^{-1}	0.001	1.0

4. Results

Fig. 2 shows the bubble of Case A2 (Ca $=$ 0.5 and Re $=$ 0.11) during its collision with the wall, along with contours of the dimensionless flow velocity u/U in x-direction, for dimensionless time $\tau \in \{-2, 0, 5, 10\}$. After an initial deformation of the bubble, a film starts to form between the bubble surface and the wall (see Fig. 2b). Once the pressure in the film is sufficiently high, a characteristic dimple forms at the top of the bubble (further discussed in Section 4.2). As the bubble continues to approach the wall, the drainage of this film becomes the dominant mechanism governing the motion of the bubble, and the shape of the bubble does no longer change noticeably. Hence, similar to the work of [3,9], two distinct collision regimes can be identified: (a) the deformation regime, where the deformation of the bubble dominates, and (b) the drainage regime, in which the drainage of the film between bubble and wall governs the bubble–wall collision. Note that the drainage of the film is clearly visible in Fig. 2c and 2d by the velocity directed tangential to the wall at the rim of the dimple. In Fig. 3a considerably larger deformation is observed for the bubble with Ca $=$ 20 than for the bubble with Ca $=$ 0.2, due to the dominance of viscous pressure over capillary pressure in the former case. The larger deformation of the bubble with higher Ca results in a thicker film separating the bubble surface and the wall (as discussed in Section 4.1) as well as in a larger radius of this film.

4.1. Bubble motion

Comparing bubbles with different fluid properties and different initial diameter d_0, a self-similar transient evolution (*i.e.* as a function of τ) of the dimensionless film thickness $\hat{h} = h/d_0$, shown in Fig. 4, as well as the dimensionless distance between the wall and the centre of mass of the bubble $\hat{l} = l/d_0$, shown in Fig. 5, is observed for bubbles with the same capillary number Ca. This similarity is observed for all considered cases given in Table 1, which includes cases in the parameter range Re $= 0.026 - 0.933$, We $= 5.084 \times 10^{-3} - 18.656$ and Mo $= 0.138 - 3.732 \times 10^{7}$. For instance, the capillary number of Cases D1 and D2 is Ca $=$ 0.5 and both cases show a similar temporal evolution of $\hat{h}$ and $\hat{l}$, despite a difference of factor 8 in Re and We, and factor 64 in Mo. Furthermore, the similarity of the bubble motion is independent of the density and viscosity ratios, ranging from $\rho_d/\rho_c = 0.001-0.99$ and $\mu_d/\mu_c = 0.01 - 1$, respectively.

The collision of a bubble with a solid wall in the creeping flow regime is, hence, governed by viscous stresses and surface tension, whereas inertia as well as the Morton number Mo have a negligible influence. This is also indicated by the Eötvös number Eo, defined in Eq. (5), which quantifies the ratio of buoyancy and surface tension but reduces to a ratio of viscosity and surface tension in the creeping flow regime, see Eq. (7). Furthermore, the observed similarity confirms t_c, Eq. (8), as the characteristic timescale of the bubble–wall collision.

4.2. Bubble shape

The self-similarity of the temporal evolution of the film thickness and the distance between the centre of mass of the bubble and the wall, reported in the previous section, is also observed for the shape of the bubble during the collision with a wall. For instance, the cross-section of bubbles with Ca $=$ 0.2 and Ca $=$ 5 are shown in Figs. 6 and 7, respectively, at $\tau \in \{0, 10, 20\}$. The same bubble shape is observed for bubbles with the same capillary number Ca. Thus, also considering the self-similarity discussed in Section 4.1, bubbles with the same capillary number Ca exhibit the same hydrodynamics irrespective of other parameters (e.g., density ratio ρ_d/ρ_c) of the two-fluid system. This is significant, for instance, for the fluid selection in experimental studies, as it allows to choose the properties of the bubble to attain a certain capillary number (*e.g.* by manipulating the surface tension coefficient with a surfactant) irrespective of other parameters.

With respect to the formation of the characteristic dimple, previous studies [14,27–29] assumed that the dimple forms when the film pressure is larger than the pressure in the bubble. Fig. 8 shows the bubble of Case A2 along with the contours of the hydrodynamic pressure $p_h = p - p_s$, where p_s is the hydrostatic pressure due to gravity, in an axisymmetric plane cutting through the centre of the bubble at the time when the dimple forms. Dimple formation is marked by a change in sign of the interface curvature κ_{top} at the top-side (*i.e.* facing the top wall) of the bubble surface. The hydrodynamic pressure in the film between the bubble and the wall is largest along the centreline of the bubble, see Fig. 8, and is increasing as the bubble approaches the wall. The pressure contours suggest that the dimple forms when the pressure in the film becomes larger than the pressure inside the bubble at the top surface of the bubble, confirming the findings and assumptions of previous studies for bubbles at Re $>$ 1 [14,27–29]. As observed

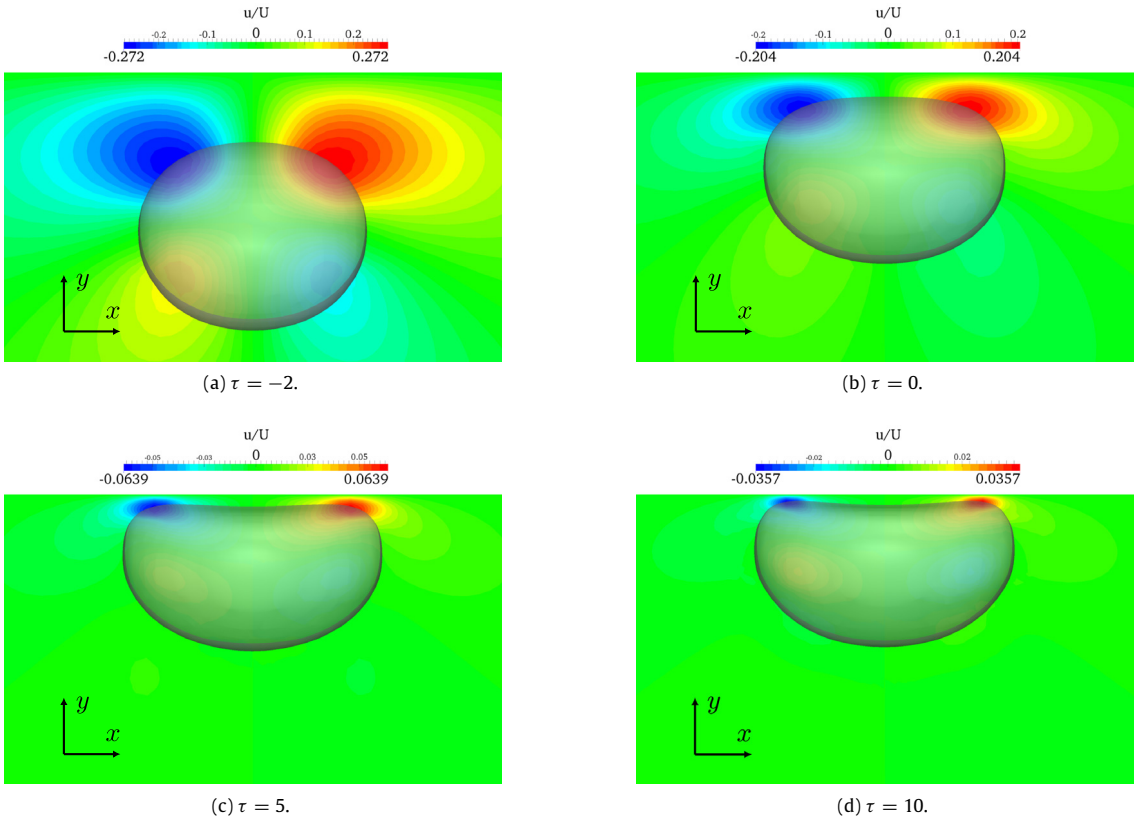

(a) $\tau = -2$. (b) $\tau = 0$.

(c) $\tau = 5$. (d) $\tau = 10$.

Fig. 2. Bubble shape and contours of the dimensionless flow velocity u/U in x-direction in the x-y plane through the centre of the bubble for Case A2 (Ca = 0.5, Re = 0.11) at different time instants τ. Note that not the entire computational domain is shown.

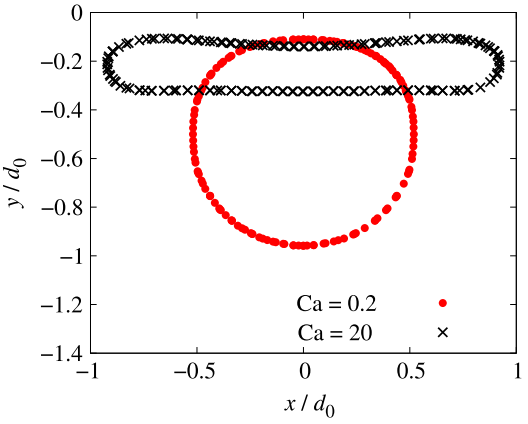

Fig. 3. Cross section of bubbles with Ca = 0.2 and Ca = 20 at dimensionless time $\tau = 0$.

in Fig. 9, the dimensionless film thickness $\hat{h}_\mathrm{p}$ at which the dimple forms can be approximated for Ca ≤ 1 as

$$\hat{h}_\mathrm{p} = \frac{h_\mathrm{p}}{d_0} \approx 0.1\,\mathrm{Ca}^{1/2}, \tag{15}$$

whereas for Ca > 1 the function

$$\hat{h}_\mathrm{p} \approx 0.19 - 0.09\,\mathrm{Ca}^{-1/2} \tag{16}$$

provides a good estimate.

4.3. Approach velocity

Previous studies (*e.g.* [3,10]) of bubble–wall and bubble-interface collisions with Re $\gg 1$ have reported a significant influence of the approach velocity of the bubble on the temporal evolution of the collision. Fig. 10 shows the dimensionless rise velocity of the bubble $\hat{u}_\mathrm{r} = u_\mathrm{r}/U$ (Fig. 10a) and the dimensionless film thickness $\hat{h}$ (Fig. 10b) as a function of dimensionless time τ of two bubbles with Ca $= 1$. As a result of the different fluid properties of the two considered cases, the bubble in Case A1 ($p_\mathrm{b} =$ 96.89 Pa) accelerates considerably faster and, hence, approaches the wall with a higher dimensionless velocity than Case B3 ($p_\mathrm{b} =$ 49.05 Pa). Despite the clearly different velocity with which the bubbles approach the wall, the rise velocity $\hat{u}_\mathrm{r}$ as well as the film thickness $\hat{h}$ for both bubbles converge at $\tau \approx 0$ and the subsequent hydrodynamics of the bubble as well as the film drainage are identical in both cases.

In the creeping flow regime the bubble–wall collision is, thus, independent of the approach velocity of the bubble and, consequently, also at which initial distance to the wall the bubble is released. This corresponds well with the role of inertia in the creeping flow regime (*i.e.* being essentially negligible) but stands in contrast to the significant influence of inertia for Re $\gg 1$ reported by Zenit and Legendre [10] and Zawala et al. [3]. The results also suggest that the characteristic velocity, Eq. (1), can be regarded as a measure of buoyancy acting on the bubble, irrespective of whether or not the bubble is actually reaching its terminal velocity.

4.4. Film drainage

Fig. 11 shows the dimensionless minimum film thickness $\hat{h}$ as a function of dimensionless time $\tau_\mathrm{f} = t/t_\mathrm{f}$, where t_f is the timescale

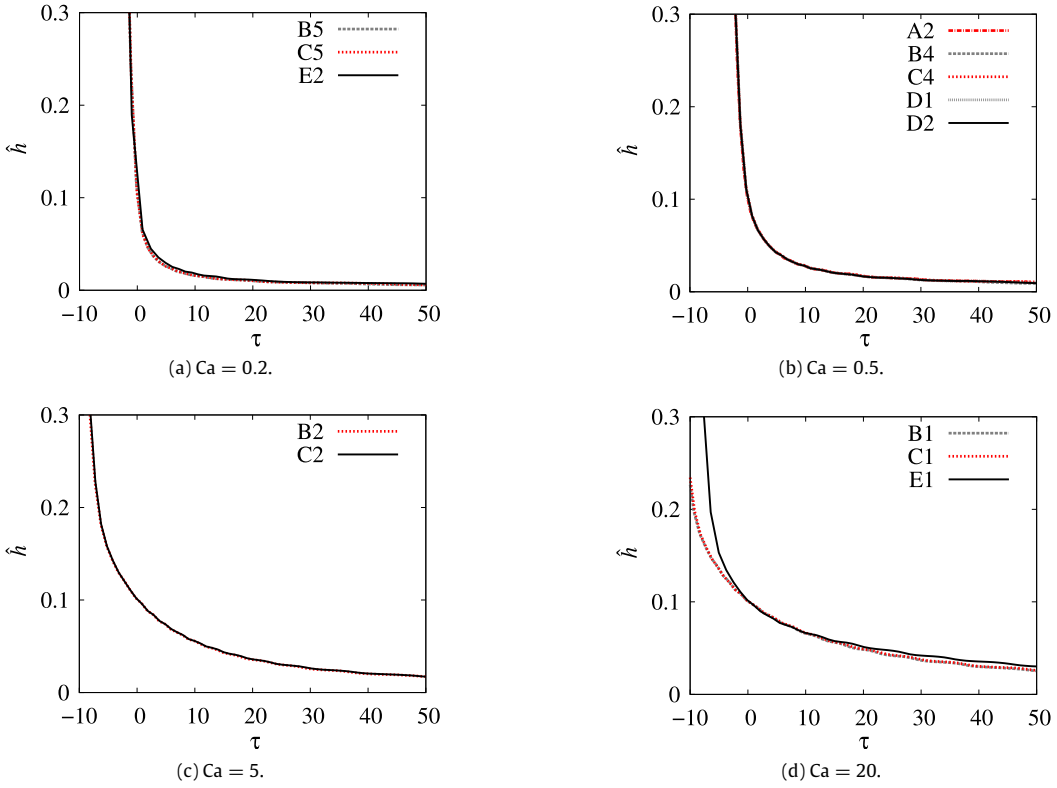

(a) Ca = 0.2. (b) Ca = 0.5.

(c) Ca = 5. (d) Ca = 20.

Fig. 4. Temporal evolution of the dimensionless film thickness $\hat{h} = h/d_0$ with respect to the dimensionless time $\tau = t/t_c$ for cases with different capillary number Ca.

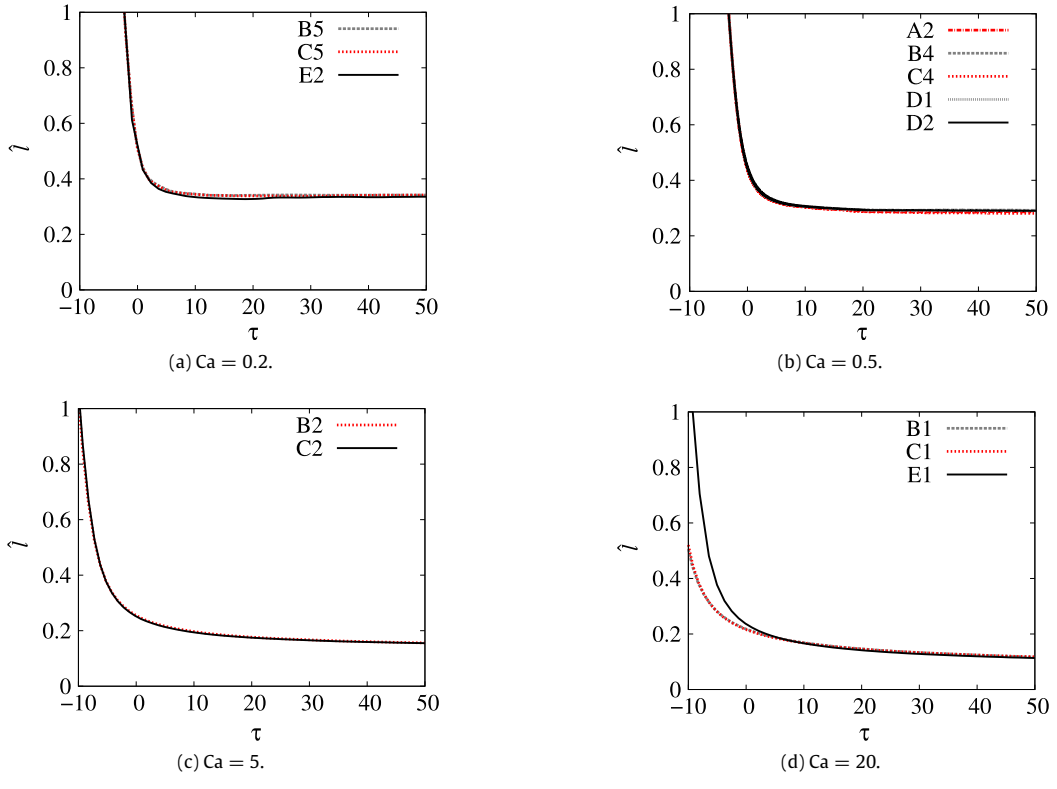

(a) Ca = 0.2. (b) Ca = 0.5.

(c) Ca = 5. (d) Ca = 20.

Fig. 5. Temporal evolution of the dimensionless distance between the centre of mass of the bubble and the wall $\hat{l} = l/d_0$ with respect to the dimensionless time $\tau = t/t_c$ for cases with different capillary number Ca.

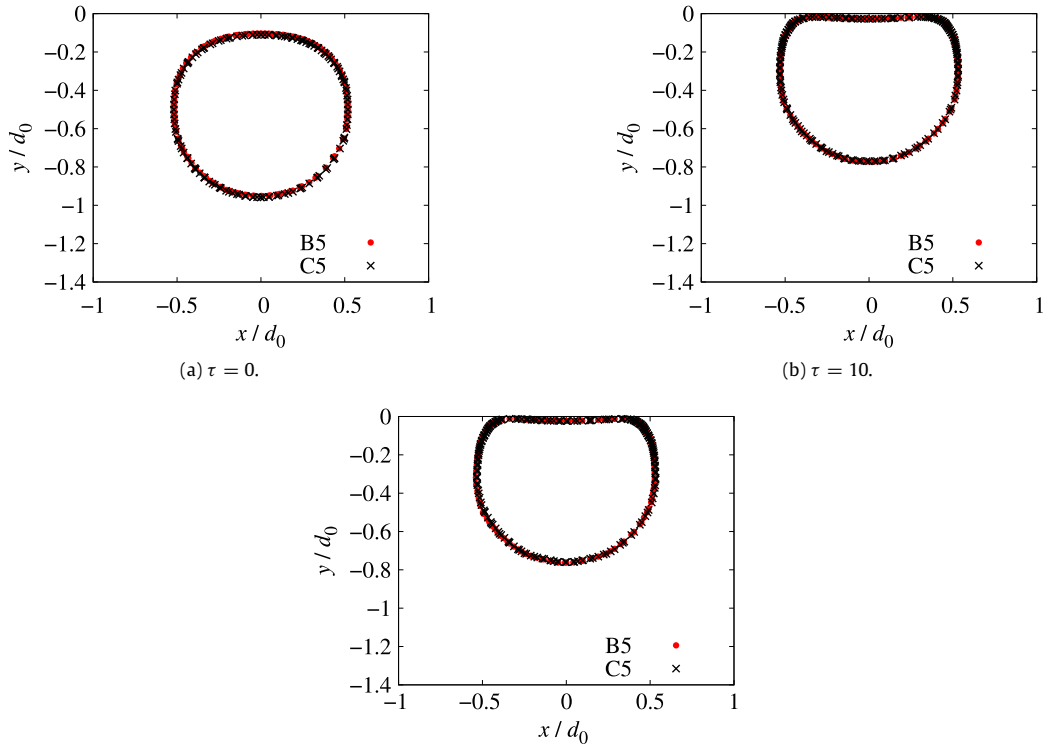

(a) $\tau = 0$.

(b) $\tau = 10$.

(c) $\tau = 20$.

Fig. 6. Cross section of bubbles with Ca = 0.2 at different instants of dimensionless time $\tau = t/t_c$.

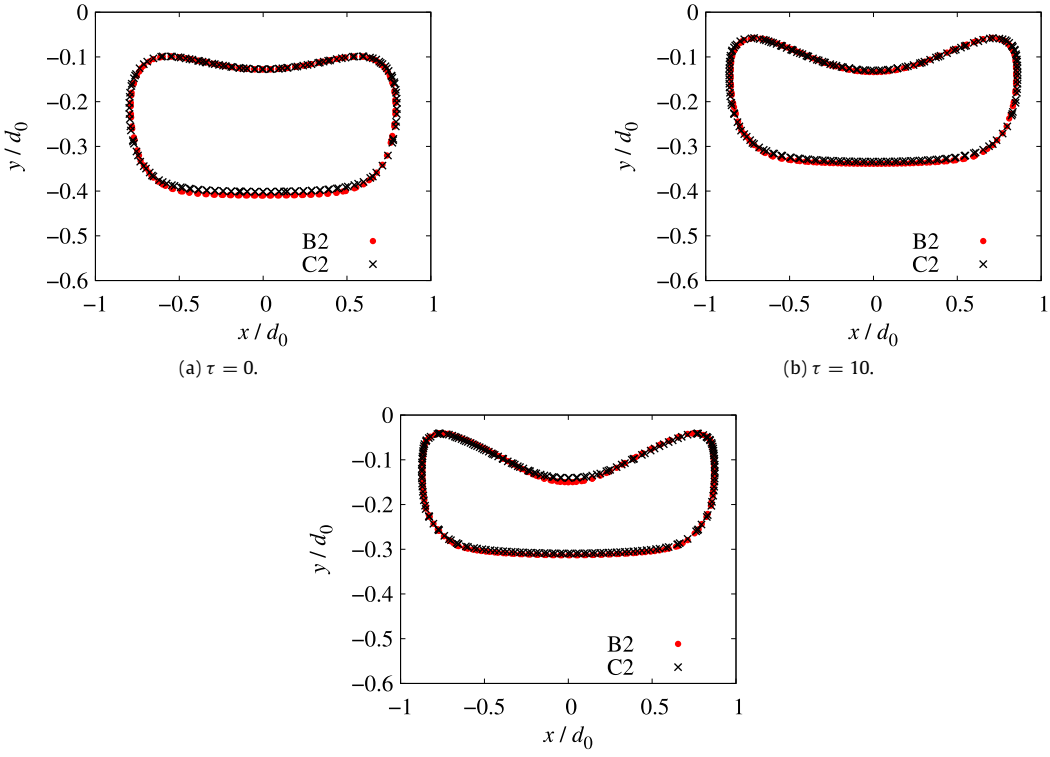

(a) $\tau = 0$.

(b) $\tau = 10$.

(c) $\tau = 20$.

Fig. 7. Cross section of bubbles with Ca = 5 at different instants of dimensionless time $\tau = t/t_c$.

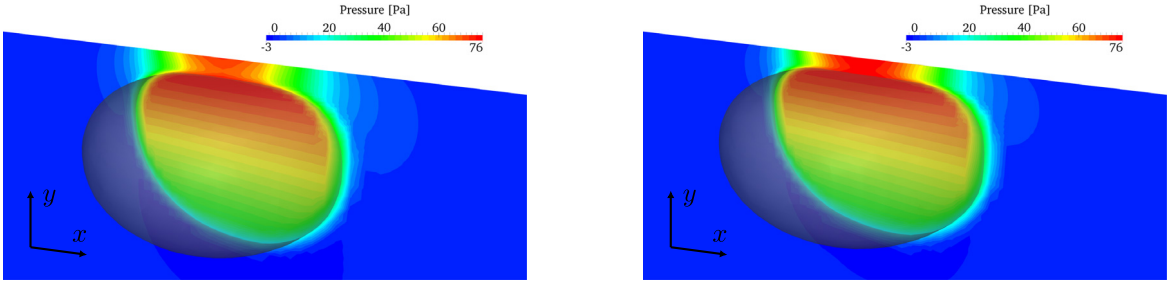

(a) $\kappa_{\text{top}} = 0.047\, d_0^{-1}$. (b) $\kappa_{\text{top}} = -0.056\, d_0^{-1}$.

Fig. 8. Contours of the hydrodynamic pressure p_{h} in the x-y plane through the centre of the bubble of Case A2 (Ca = 0.5, Re = 0.11) for time instants just before and after the formation of the dimple (where $\kappa_{\text{top}} = 0$). Note that the plane is tilted to better visualise the pressure field and that not entire computational domain is shown.

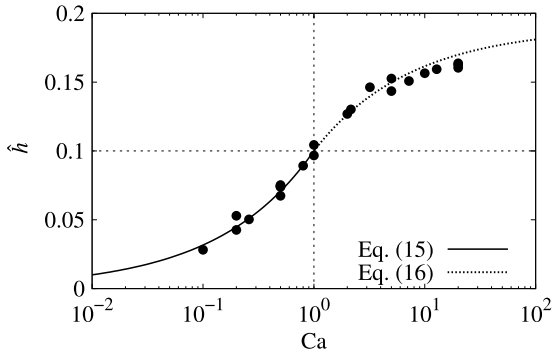

Fig. 9. Dimensionless film thickness $\hat{h} = h/d_0$ at which the formation of the dimple is observed (*i.e.* $\kappa_{\text{top}} = 0$) for all considered cases. Note that also the results of additional cases are shown here which are not explicitly mentioned in Table 1 or discussed in any of the previous sections.

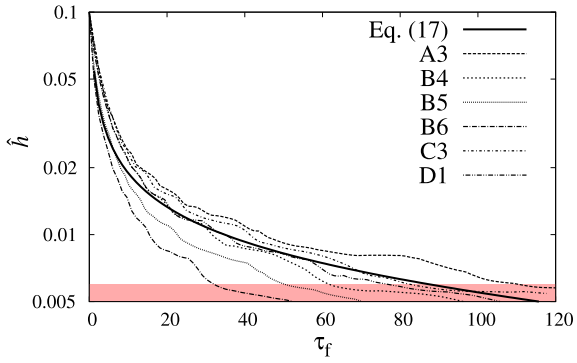

Fig. 11. Temporal evolution of the dimensionless film thickness $\hat{h} = h/d_0$ with respect to the dimensionless drainage time $\tau_{\text{f}} = t/t_{\text{f}}$ for cases with different capillary number Ca, along with the function given in Eq. (17). The shaded region for $\hat{h} \leq 0.006$ illustrates the film thickness for which the simulation results become unreliable, due to the available mesh resolution.

of the film drainage proposed by Chan et al. [27], given in Eq. (9). All considered cases follow the same trend and the temporal evolution of the film thickness can be approximated as

$$\hat{h} \approx \mathcal{A}\, \tau_{\text{f}}^{-1/2} + \mathcal{B}\, \tau_{\text{f}}, \tag{17}$$

with $\mathcal{A} = 6 \times 10^{-2}$ and $\mathcal{B} = -5 \times 10^{-6}$ for the presented results. Thus, the timescale t_{f} provides a reference timescale of the drainage time for the purpose of comparing the influence of different fluid properties and bubble sizes. Inserting the equations for the capillary number Ca, see Eq. (3), and the characteristic velocity U, see Eq. (1), the timescale of the film drainage given by Eq. (9) becomes

$$t_{\text{f}} = \mu_{\text{c}} \sqrt{\frac{6\,\Lambda}{\sigma\, g\, \Delta\rho}}. \tag{18}$$

Thus, the timescale of the film drainage is independent of the size of the bubble and is only dependent on the fluid properties.

As seen in Fig. 3, the increase in Ca for a larger bubble results in a larger deformation of the bubble and a thicker film, which increases viscous dissipation in the film and leads to a longer drainage time. However, the large size of the bubble also leads to a larger buoyancy force, which causes an increase of the drainage

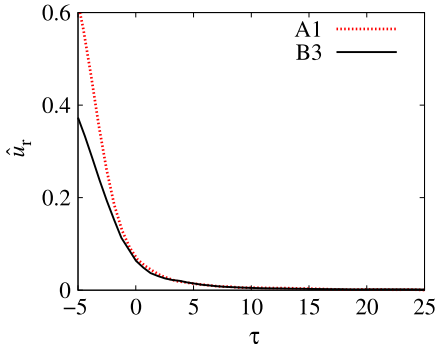

(a) Rise velocity $\hat{u}_{\text{r}}$.

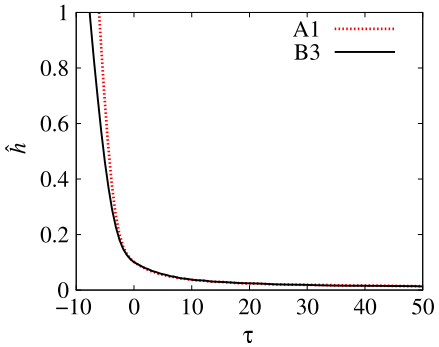

(b) Film thickness $\hat{h}$.

Fig. 10. Temporal evolution of the dimensionless rise velocity of the bubble $\hat{u}_{\text{r}} = u_{\text{r}}/U$ and the dimensionless film thickness $\hat{h} = h/d_0$ with respect to the dimensionless time $\tau = t/t_{\text{c}}$ for cases with capillary number Ca = 1.

rate of the film. Thus, the larger film radius and the increase in buoyancy force are balancing each other and eliminate the influence of the size of the bubble on the drainage of the film for a given set of fluid properties. This stands in contrast to bubble–wall collisions in the creeping flow regime when the bubble deformation is negligible, such as the bubble–wall collision of an air bubble in water in the creeping flow regime. Parkinson and Ralston [25] reported experimental results of an air bubble rising in water with $\mathrm{Re} < 1$, where during the collision of that bubble with a solid wall the drainage time of the film was found to increase with increasing bubble size due to the increase in buoyancy force. Hence, the deformation of the bubble during the collision has a strong influence on the film drainage.

Since the bubble is moving at a significantly reduced speed once it has transitioned into the drainage regime, it is expected (although not explicitly studied here) that the approximation given in Eq. (17) also holds and the timescale of the film drainage is also independent of the bubble size even for bubbles with $\mathrm{Re} > 1$, despite Eq. (3) for the characteristic velocity being strictly speaking only valid in the creeping flow regime ($\mathrm{Re} < 1$).

5. Conclusions

A systematic study of the collision of a gravity-driven bubble with a horizontal wall in the creeping flow regime ($\mathrm{Re} < 1$) has been conducted. The analysis of the presented results for bubbles spanning a wide range of relevant parameters unveils a self-similarity with respect to the capillary number of the bubble shape as well as the film thickness between the bubble and the wall. This self-similarity has been shown to be independent of the fluid properties of the two-phase system as well as independent of the (terminal) Reynolds number or approach velocity of the bubble. Interestingly, given the observed behaviour and similarity is unaltered in the wide range of considered Morton numbers ($\mathrm{Mo} = 10^{-1}$–10^{7}), suggests that the Morton number, one of the dimensionless groups used to parameterise the buoyancy-driven rise of a bubble [40], is irrelevant for the characterisation of the bubble–wall collision.

When the pressure in the film between the bubble surface and the wall becomes higher than the pressure inside the bubble, a characteristic dimple forms at the top of the bubble. This is in agreement with findings reported in previous studies related to bubbles with $\mathrm{Re} \gg 1$. The film thickness at which this dimple forms was found to be a function of the capillary number, as dictated by the reported self-similarity of the bubble shape and the film thickness. With regards to the drainage of the film, the dimensionless film thickness was shown to correlate with the timescale of the film drainage for the considered cases. Interestingly, this timescale is independent of the size of the bubble and is only dependent on the fluid properties. A correlation for the dimensionless film thickness as a function of the timescale of the film drainage has been proposed based on the simulation results, that allows an *a priori* estimation of the drainage time of the bubble–wall collision for a given two-phase system. Crucially, since the Reynolds number of the film drainage is typically $\mathrm{Re_f} < 1$ even for bubbles with $\mathrm{Re} \gg 1$, the findings associated with the film drainage are also expected to apply to bubbles outside the remit of the creeping flow regime.

In summary, all studied aspects of the hydrodynamics of the wall collision of a deformable bubble in the creeping flow regime are correlated with the capillary number, revealing a dominant influence of the viscocapillary balance on the bubble–wall collision. Inertia has a negligible influence on the bubble–wall collision, which fits well into the general characteristics of the creeping flow regime. The presented results extend the findings of Abid and Chesters [32], who previously reported a similarity associated with the capillary number for drop–drop collisions in the limit of small interface deformation as well as assuming a plug velocity profile in the film separating both drops and neglecting the effect of the film drainage on the pressure field. It can, therefore, be concluded that the nonlinearity introduced by the considerable deformation of the fluid interface as well as the local velocity field and pressure distribution have no discernible influence on the scaling and similarity of the bubble–wall collision in the creeping flow regime. The presented findings confirm that foams can form in pure (uncontaminated) fluids, as previously observed experimentally [1,46], contrary to the widely proclaimed notion that pure liquids cannot foam [2]; in fact, whether a foam forms depends on the observed timescale. In practice, this is particularly relevant for very viscous fluids, such as lubricant oil or molten glass, for which the bubble Reynolds numbers are small for a wide range of bubble sizes and for which the film drainage occurs over a practically significant timespan. To this end, the presented results, and particularly the proposed correlation for the film drainage, can be used to distinguish viscous drainage that occurs regardless of the surface-active contamination of the interface.

Acknowledgements

The financial support from the Engineering and Physical Sciences Research Council (EPSRC) through Grant No. EP/M021556/1 is gratefully acknowledged. Data supporting this publication can be obtained from https://doi.org/10.5281/zenodo.95946 under a Creative Commons Attribution license.

References

[1] T. Sanada, M. Watanabe, T. Fukano, Effects of viscosity on coalescence of a bubble upon impact with a free surface, Chem. Eng. Sci. 60 (2005) 5372–5384.
[2] K. Malysa, K. Lunkenheimer, Foams under dynamic conditions, Curr. Opin. Colloid Interface Sci. 13 (2008) 150–162.
[3] J. Zawala, S. Dorbolo, N. Vandewalle, K. Malysa, Bubble bouncing at a clean water surface, Phys. Chem. Chem. Phys. 15 (2013) 17324–17332.
[4] R. Yoon, The role of hydrodynamic and surface forces in bubble-particle interaction, Int. J. Miner. Process. 58 (2000) 129–143.
[5] D. Donoghue, Y. Delauré, A. Albadawi, A. Robinson, D. Murray, Bouncing bubble dynamics and associated enhancement of heat transfer, J. Phys. Conf. Ser. 395 (2012) 012167.
[6] D. Donoghue, A. Albadawi, Y. Delauré, A. Robinson, D. Murray, Bubble impingement and the mechanisms of heat transfer, Int. J. Heat Mass Transfer 71 (2014) 439–450.
[7] H.-K. Tsao, D.L. Koch, Observations of high Reynolds number bubbles interacting with a rigid wall, Phys. Fluids 9 (1997) 44.
[8] K. Malysa, M. Krasowska, M. Krzan, Influence of surface active substances on bubble motion and collision with various interfaces, Adv. Colloid Interface Sci. 114–115 (2005) 205–225.
[9] J. Zawala, M. Krasowska, T. Dabros, K. Malysa, Influence of bubble kinetic energy on its bouncing during collisions with various interfaces, Can. J. Chem. Eng. 85 (2007) 669–678.
[10] R. Zenit, D. Legendre, The coefficient of restitution for air bubbles colliding against solid walls in viscous liquids, Phys. Fluids 21 (2009) 1–12.
[11] M.H.W. Hendrix, R. Manica, E. Klaseboer, D.Y.C. Chan, C.-D. Ohl, Spatiotemporal evolution of thin liquid films during impact of water bubbles on glass on a micrometer to nanometer scale, Phys. Rev. Lett. 108 (2012) 247803.
[12] J. Zawala, T. Dabros, Analysis of energy balance during collision of an air bubble with a solid wall, Phys. Fluids 25 (2013) 123101.
[13] A. Albadawi, D. Donoghue, A. Robinson, D. Murray, Y. Delauré, On the assessment of a vof based compressive interface capturing scheme for the analysis of bubble impact on and bounce from a flat horizontal surface, Int. J. Multiph. Flow. 65 (2014) 82–97.
[14] R. Manica, M.H.W. Hendrix, R. Gupta, E. Klaseboer, C.D. Ohl, D.Y.C. Chan, Modelling bubble rise and interaction with a glass surface, Appl. Math. Model. 38 (2014) 4249–4261.
[15] J. Zawala, K.M. Kosior, Formation and influence of the dynamic adsorption layer on kinetics of the rising bubble collisions with solution/gas and solution/solid interfaces, Adv. Colloid Interface Sci. 222 (2014) 765–778.
[16] R. Manica, E. Klaseboer, D.Y.C. Chan, Force balance model for bubble rise, impact, and bounce from solid surfaces, Langmuir 31 (2015) 6763–6772.
[17] M. Krzan, K. Lunkenheimer, K. Malysa, Pulsation and bouncing of a bubble prior to rupture and/or foam film formation, Langmuir 19 (2003) 6586–6589.

[18] D. Legendre, C. Daniel, P. Guiraud, Experimental study of a drop bouncing on a wall in a liquid, Phys. Fluids 17 (2005) 097105.
[19] F. Suñol, R. González-Cinca, Rise, bouncing and coalescence of bubbles impacting at a free surface, Colloids Surf. A 365 (2010) 36–42.
[20] E. Manev, A. Nguyen, Critical thickness of microscopic thin liquid films, Adv. Colloid Interface Sci. 114–115 (2005) 133–146.
[21] E. Manev, J. Angarska, Critical thickness of thin liquid films: Comparison of theory and experiment, Colloids Surf. A 263 (2005) 250–257.
[22] B. Dai, L. Leal, A. Redondo, Disjoining pressure for nonuniform thin films, Phys. Rev. E 78 (2008) 1–9.
[23] S. Karakashev, E. Manev, Hydrodynamics of thin liquid films: Retrospective and perspectives, Adv. Colloid Interface Sci. 222 (2015) 398–412.
[24] E. Ruckenstein, A. Sharma, A new mechanism of film thinning: enhancement of Reynolds' velocity by surface waves, J. Colloid Interface Sci. 119 (1987) 1–13.
[25] L. Parkinson, J. Ralston, The interaction between a very small rising bubble and a hydrophilic titania surface, J. Phys. Chem. C 114 (2010) 2273–2281.
[26] P. Kruglyakov, S. Karakashev, A. Nguyen, N. Vilkova, Foam drainage, Current Opinion in Colloid and Interface Science 13 (2008) 163–170.
[27] D.Y.C. Chan, E. Klaseboer, R. Manica, Film drainage and coalescence between deformable drops and bubbles, Soft Matter 7 (2011) 2235–2264.
[28] R. Manica, M. Hendrix, R. Gupta, E. Klaseboer, C.-D. Ohl, D. Chan, Effects of hydrodynamic film boundary conditions on bubble–wall impact, Soft Matter 9 (2013) 9755–9758.
[29] E. Klaseboer, R. Manica, M.H.W. Hendrix, C.-D. Ohl, D.Y.C. Chan, A force balance model for the motion, impact, and bounce of bubbles, Phys. Fluids 26 (2014) 092101.
[30] R. Manica, E. Klaseboer, D. Chan, The hydrodynamics of bubble rise and impact with solid surfaces, Adv. Colloid Interface Sci. (2016) 1–21.
[31] E. Klaseboer, J. Chevaillier, C. Gourdon, O. Masbernat, Film drainage between colliding drops at constant approach velocity: Experiments and modeling, J. Colloid Interface Sci. 229 (2000) 274–285.
[32] S. Abid, A. Chesters, The drainage and rupture of partially-mobile films between colliding drops at constant approach velocity, Int. J. Multiph. Flow. 20 (1994) 613–629.
[33] E. Ascoli, D. Dandy, L. Leal, Buoyancy-driven motion of a deformable drop toward a planar wall at low Reynolds number, J. Fluid Mech. 213 (1989) 287.
[34] J. Blawzdziewicz, R. Goodman, N. Khurana, E. Wajnryb, Y.-N. Young, Nonlinear hydrodynamic phenomena in Stokes flow regime, Physica D 239 (2010) 1214–1224.
[35] E. Becker, W. Hiller, T. Kowalewski, Experimental and theoretical investigation of large-amplitude oscillations of liquid droplets, J. Fluid Mech. 231 (1991) 189–210.
[36] F. Denner, G. Paré, S. Zaleski, Dispersion and viscous attenuation of capillary waves with finite amplitude, Eur. Phys. J. Spec. Top. 226 (2017) 1229–1238.
[37] F. Denner, B. van Wachem, Fully-coupled balanced-force VOF framework for arbitrary meshes with least-squares curvature evaluation from volume fractions, Numer. Heat Transfer B 65 (2014) 218–255.
[38] F. Denner, B. van Wachem, Compressive VOF method with skewness correction to capture sharp interfaces on arbitrary meshes, J. Comput. Phys. 279 (2014) 127–144.
[39] G.K. Batchelor, An Introduction to Fluid Dynamics, Cambridge University Press, New York, 1967.
[40] J. Grace, Shapes and velocities of bubbles rising in infinite liquids, Trans. Inst. Chem. Eng. 51 (1973) 116–120.
[41] F. Denner, D. van der Heul, G. Oud, M. Villar, A. da Silveira Neto, B. van Wachem, Comparative study of mass-conserving interface capturing frameworks for two-phase flows with surface tension, Int. J. Multiph. Flow. 61 (2014) 37–47.
[42] C. Hirt, B. Nichols, Volume of fluid (VOF) method for the dynamics of free boundaries, J. Comput. Phys. 39 (1981) 201–225.
[43] J. Brackbill, D. Kothe, C. Zemach, Continuum method for modeling surface tension, J. Comput. Phys. 100 (1992) 335–354.
[44] F. Denner, Frequency dispersion of small-amplitude capillary waves in viscous fluids, Phys. Rev. E 94 (2016) 023110.
[45] F. Denner, B. van Wachem, Numerical time-step restrictions as a result of capillary waves, J. Comput. Phys. 285 (2015) 24–40.
[46] H. Caps, G. Delon, N. Vandewalle, R. Guillermic, O. Pitois, A.L. Biance, L. Saulnier, P. Yazhgur, E. Rio, A. Salonen, D. Langevin, Does water foam exist in microgravity? Europhys. News 45 (2014) 22–25.